Case Studies in Thermal Engineering 12 (2018) 644–654

Contents lists available at ScienceDirect

Case Studies in Thermal Engineering

journal homepage: www.elsevier.com/locate/csite

# Bree's diagram of a functionally graded thick-walled cylinder under thermo-mechanical loading considering nonlinear kinematic hardening

Mohsen Damadam[a], Reza Moheimani[b,*], Hamid Dalir[c]

[a] The Neil Armstrong Hall of Engineering, Purdue University, West Lafayette, IN 47907, USA
[b] School of Mechanical Engineering, Purdue University, West Lafayette, IN 47907, USA
[c] Department of Mechanical and Energy Engineering, Purdue School of Engineering and Technology, Indianapolis, IN 46202, USA

ARTICLE INFO

*Keywords:*
Functionally graded material
Nonlinear kinematic hardening
Thermal/mechanical stress
Return mapping algorithm
Shakedown
Ratcheting
Bree's diagram

ABSTRACT

In this paper, elasto-plastic analysis of a thick-walled cylinder made of functionally graded materials (FGMs) subjected to constant internal pressure and cyclic temperature gradient loading is carried out using MATLAB. The material is assumed to be isotropic and independent of temperature with constant Poisson's ratio and the material properties vary radially based on a power law volume function relation. The Von Mises' yield criterion and the Armstrong-Frederick nonlinear kinematic hardening model were implemented in this investigation. To obtain the incremental plastic strain, return mapping algorithm (RMA) was used. At the end, the Bree's interaction diagram is plotted in terms of non-dimensional pressure and temperature which represents an engineering index for optimum design under thermo-mechanical loading.

## 1. Introduction

Strain measurement at raised temperatures is vital for the investigation of specific thermo-mechanical properties of materials employed in high-temperature environment. This is effectively of interest in the energy sector (such as gas turbines and steam pipelines) where hot parts need highly maintenance to extend their life as they operate at high temperature and pressure. To deal with thermomechanical loads, a novel generation of engineered materials are needed. A functionally graded material (FGM) has increasingly been used in the thermo-elasto-plastic analyses. The thermomechanical properties of FGM exhibit a smooth and continuous change through the thickness of structure, thus mitigating thermal stress concentration and eliminating interface debonding problems, often being observed in laminated composite structures. The mentioned advantage of FG material is achieved by gradually altering over the volume fraction of bulk materials which are generally consisting of metal and ceramic parts. The ceramic constituents of FGMs are capable of withstanding high-temperature environments for better thermal fatigue resistance characteristics, while the metal constituents provide stronger mechanical performance and reduce the possibility of catastrophic fracture [1].

Numerous applications in dental implant, aerospace, gears, turbine rotors etc., have made this new class of engineered material much more attentive to scientists. Hence, new methodologies must be developed to analyze stress-strain response and design FGMs [2,3].

Recently, some studies have been carried out on thermo-mechanical analyses of various structures. Jalali et al. [4,5] presented free vibration analysis of rotating FG annular disk of in thermal environment. It was shown that by increasing the temperature change

* Corresponding author.
*E-mail address:* rezam@purdue.edu (R. Moheimani).

https://doi.org/10.1016/j.csite.2018.08.004
Received 9 June 2018; Received in revised form 19 July 2018; Accepted 21 August 2018
Available online 22 August 2018

in the microbeam, the natural frequencies decreased, and results could improve the design of the rotating FG disk in order to avoid resonance condition. Khoei and Bahmani [6] presented a formulation for the pressure-dependent thermo-mechanical contact problem using the X-FEM method. A staggered approach based on the Newton–Raphson method was developed to show the effect of thermal contact in fracture modeling. The governing equations of a FGM Timoshenko beam resting on a non-linear strain foundation are derived and numerically solved by Sun et al. [7]. According to a power law function, they investigated thermal buckling and post buckling responses of the FGM beam with the assistance of shooting method.

Hosseini et al. [8] developed an asymmetric elastic-plastic-creep constitutive model for representation of thermo-mechanical response of cast irons under monotonic and cyclic loading conditions. The model was capable of effectively implementation to different Finite element (FE) packages. Effect of thermal gradient load on thermo-elastic vibrational behavior sandwich plates with FG nanocomposite face sheets was also investigated by Safaei et al. [9].

Using Tresca's yield criterion and its associated flow rule, Bland [10] determined the deformation of a thick-walled tube of work hardening material subjected to internal and external pressures. Derington [11] studied the principal stresses in a long elastic cylinder subjected to uniform internal or external pressure and steady state heat flow under a variety of loading conditions incorporating Tresea's yield criterion with no change of elastic constants with temperature. The effects of the gradation of strength and deformation of thick walled Functionally Graded (FG) tubes under internal pressure was investigated by Fukui and Yamanaka [12]. Obata and Noda [13] investigated the thermal stresses in a FGM hollow sphere and hollow circular cylinder. They also studied the effect of inner radius on the resulting stresses. Using incremental theory of plasticity method for thick walled cylindrical pressure vessels, Loghman and Wahab [14] obtained the plastic strain, plastic stress, and plastic zone progress for different loading conditions and thickness ratios.

An exact solution for one-dimensional thermal stresses of FGM spheres [15] and cylinders [16] presented by Lutz and Zimmerman who considered variation of Young's modulus and the thermal expansion coefficient along the radius. Shabana and Nods [17] obtained the elastoplastic thermal stresses in a functionally graded rectangular plate subjected to different kinds of temperature conditions using finite element method. Tutuncu and Ozturk [18] presented the closed-form solutions for stresses and displacements in functionally graded cylindrical and spherical vessels subjected to internal pressure alone, using the infinitesimal theory of elasticity.

Nayebi and Abdi [19] developed a numerical program to investigate the steady state behavior of thick walled spherical and cylindrical pressure vessels using linear kinematic hardening in the plastic condition and a Norton power law in the creep condition. Oral and Anlas [20] obtained closed form solutions for stress distribution in a nonhomogeneous anisotropic FG cylindrical body and compared the results with FE results.

Safari et al. [21] investigated dynamic characteristics of a FGM thick hollow cylinder under thermal shock loading. Dynamic thermo-elastic equation of the problem was analytically solved by employing the Laplace transform and series solution across the thickness of cylinder. They obtained a good agreement between obtained results of presented method and published data.

You et al. [22] analyzed the steady state creep in thick walled FGMs cylinders subjected to internal pressure. The impact of radial variations of material parameters on the stresses in the cylinder was also investigated. Reddy and Chin [23] studied the dynamic thermos-elastic response of functionally graded cylinders. They used first order shear deformation plate theory and developed a finite element model of the formulation.

Chen et al. [24] investigated the creep effect of thick-walled FGM cylinders subjected to both internal and external pressures. They gained the approximate solutions on the basis of a Taylor expansion series and compared it with the results of Finite Element analysis (FEA) obtained by using ABAQUS software. Abrinia et al. [25] obtained analytical solution to give solutions for FGM hollow cylindrical vessels that are under the influence of internal pressure and an arbitrary steady state temperature field. They obtained the optimum value of β, an arbitrary value affecting the stresses in the cylinder, and studied the effect of non-homogeneity in FGM thick cylinder.

Darijani et al. [26] derived an exact elasto-plastic analytical solution for a thick walled cylindrical vessel made of elastic linear-hardening material by considering the Bauschinger effect and Tresca's yield criterion. They determined best Autofrettage pressure and showed that the design of vessels based on the elasto-plastic methods is much more economic than elastic methods. Using a new approach completely different from the previous methods for solving a Fredholm integral equation Peng and Li [27] investigated the influence of the gradient variation of the material properties on thermal stresses and found that appropriate gradient can make the distribution of thermal stresses gentler in the whole structure. Naghdabadi et al. [28] obtained an analytical elastic-plastic solution for thick walled cylinders made of functionally graded materials. They developed a mathematical model to predict yielding through the thickness. Bayat et al. [29] accomplished a thermo-mechanical analysis of functionally graded hollow sphere subjected to mechanical loadings and one-dimensional steady-state thermal stresses and compared the solutions with finite element results. Steady state creep in a functionally graded thick-walled cylinder subjected to internal pressure was investigated by Singh and Singh [30]. Nayebi et al. [31] studied how continuum damage mechanics affect the behavior of a FG rotating disk. Nami et al. [32] analyzed thermal buckling of functionally graded rectangular nanoplates considering two types of uniform and nonuniform temperature distributions. Mahdavi et al. [33] studied the thermo-mechanical behavior of a FGM rotating disk with variable thickness and constant angular velocity using a power law for material properties along the radius. They compared the results with FEM and showed that the temperature dependent material properties of FGM has significant effect on the values of stress.

In the present paper, a thick-walled FG cylinder subjected to internal pressure and temperature gradient loading under plane strain condition is studied. The novelty of this work is to solve the problem numerically for a functionally graded material using return mapping algorithm and nonlinear kinematic hardening model. In addition, the well-known Bree's diagram used for designing is plotted to show the material behavior under different conditions of loadings.

## 2. Mathematical formulation

Through this study, inner surface of the cylinder is assumed to be metal and outer one ceramic. Distribution of the material properties is based on the following volume fraction model [31]:

$$f(r) = VB_o + (1-V)B_i V = \left(\frac{r - r_i}{\frac{r_o}{a} - r_i}\right)^n r_{in} \le r_{out} \tag{1}$$

where $B$ is a material property such that $B_i$ and $B_o$ are the material properties of the inner, $r_{in}$, and outer radii, $r_{out}$, respectively and n ($n \ge 0$) is the gradient parameter index. A parameter is presented such as ($0<a \le 1$) to be able to decrease the volume fraction of ceramic in the outer layer of the disk. Due to the brittleness of ceramic, it is aimed not to have 100% of it in the outer layer [32]. Elastic modulus, heat conduction coefficient, thermal coefficient of expansion, yield stress and the nonlinear kinematic hardening constants follow Eq. (1), except Poisson's ratio which is assumed to be constant; however, it varies in a very small range.

## 3. Thermal solution

For a steady state heat conduction problem considering axisymmetric conditions without internal heat generation, we have:

$$\frac{d}{dr}\left(K(r)r\frac{dT}{dr}\right) = 0 \tag{2}$$

where $K(r)$ is the heat conductivity varying according to Eq. (1) and $T(r)$ is the temperature distribution along the radius. Differentiating the above relation, the following differential equation is obtained:

$$F_1(r)T''(r) + F_2(r)T'(r) = 0 \tag{3}$$

where

$$F_1(r) = rK(r) and F_2(r) = K(r) + r\frac{dK(r)}{dr} \tag{4}$$

Finding an analytical solution for Eq. (3) is difficult. So, a semi-analytical method is implemented in this investigation. In this method, the cylinder is divided into $m$ sub-domains where $t$ denotes the radial width of each sub-domain. Calculating the coefficients of Eq. (3) at $r = r^k$ (mean radius of the $k^{th}$ division), leads to an ordinary differential equation with constant coefficients which is valid within the $k^{th}$ sub-domains. [See Fig. 1].

Solving the above differential equation [Eq. (3)]:

$$T^k = Y_1^k + Y_2^k \exp(-rF_2^k/F_1^k) \tag{5}$$

where $Y_1^k$ and $Y_2^k$ are unknown constants for $k^{th}$ sub-domain determined by applying boundary conditions between each two adjacent sub-domains. Temperature in the inner and outer surfaces of the cylinders are as follows:

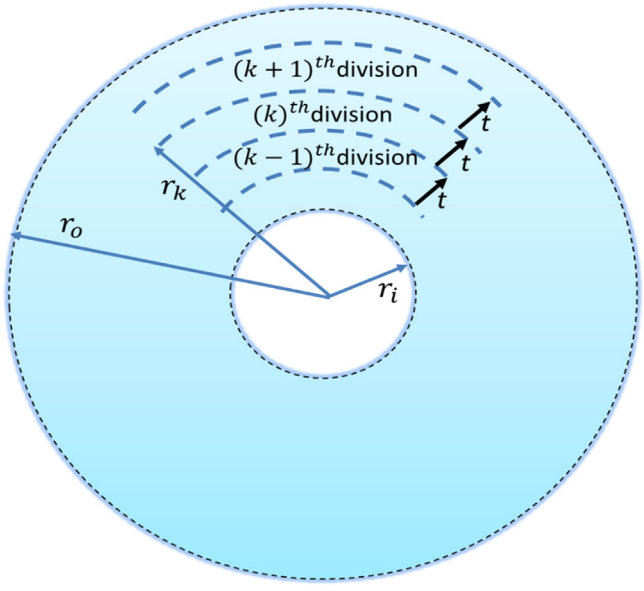


**Fig. 1.** Dividing the thick-walled cylindrical with denomination of the radii domain into some finite sub-domains [34].

$$T(r_i) = T_i \text{and} T(r_o) = 0 \tag{6}$$

The continuity of temperature and its gradient at the interfaces of the adjacent sub-domains are as follows:

$$T^k\Big|_{r=r^k+\frac{t}{2}} = T^{k+1}\Big|_{r=r^{k+1}-\frac{t}{2}} \tag{7}$$

$$\frac{dT^k}{dr}\Big|_{r=r^k+\frac{t}{2}} = \frac{dT^{k+1}}{dr}\Big|_{r=r^{k+1}-\frac{t}{2}} \tag{8}$$

Using the continuity conditions between each two adjacent sub-domains and thermal boundary conditions in inner and outer domains, yield a set of linear algebraic equations in terms of $Y_1^k$ and $Y_2^k$. Solving these equations for $Y_1^k$ and $Y_2^k$ and substituting them in relation (5), temperature distribution is obtained for all layers.

## 4. Elastic deformation

For the state of plane strain ($\varepsilon_z = 0$) and infinitesimal deformations, stresses can be obtained in the cylindrical coordinate system as follows:

$$\sigma_r = \frac{E(r)}{(1+\nu)(1-2\nu)}[(1-\nu)\varepsilon_r + \nu\varepsilon_\theta - (1+\nu)\alpha(r)T(r)] \tag{9}$$

$$\sigma_\theta = \frac{E(r)}{(1+\nu)(1-2\nu)}[\nu\varepsilon_r + (1-\nu)\varepsilon_\theta - (1+\nu)\alpha(r)T(r)] \tag{10}$$

$$\sigma_z = \nu(\sigma_r + \sigma_\theta) - E(r)\alpha(r)T(r) \tag{11}$$

where E is the Young's modulus, $\nu$ Poisson's ratio and $\alpha$ the coefficient of thermal expansion.

For an axisymmetric hollow cylinder, components of strain can be calculated from the following geometric relations:

$$\varepsilon_r = \frac{du}{dr} \quad , \quad \varepsilon_\theta = \frac{u}{r} \tag{12}$$

with u being the displacements in r direction and substituting the radial and circumferential stresses in terms of displacement into the following equilibrium equation

$$\frac{d}{dr}(r\sigma_r) - \sigma_\theta = 0 \tag{13}$$

We obtain an equation in terms of radial displacement (Navier equation) as:

$$C_1(r)\frac{d^2u}{dr^2} + C_2(r)\frac{du}{dr} + C_3(r)u + C_4(r) = 0 \tag{14}$$

in which $C_1$ to $C_4$ are:

$$C_1(r) = \frac{rE(r)}{1+\nu} \tag{15}$$

$$C_2(r) = \frac{E(r)}{1+\nu} + \frac{r}{1+\nu}\frac{dE(r)}{dr} \tag{16}$$

$$C_3(r) = \frac{\upsilon}{1-\upsilon^2}\frac{dE(r)}{dr} - \frac{E(r)}{r(1+\nu)} \tag{17}$$

$$C_4(r) = \frac{-r}{1-\nu}\frac{d}{dr}(E(r)\alpha(r)T(r)) \tag{18}$$

## 5. Plastic deformation

In the plastic model, plastic strains are emerged in governing equations. So, we can capture total strain as below.

$$\varepsilon_{ij} = \varepsilon_{ij}^M + \varepsilon_{ij}^T + \varepsilon_{ij}^P \tag{19}$$

where M, T, and P index denote mechanical, thermal, and plastic conditions respectively. Using Hooke's law, stresses are obtained in terms of strains.

$$\sigma_r = \frac{E(r)}{(1+\nu)(1-2\nu)}[(1-\nu)\varepsilon_r + \nu\varepsilon_\theta - (1-\nu)\varepsilon_r^p - \nu\varepsilon_\theta^p - \nu\varepsilon_z^p - (1+\nu)\alpha(r)T(r)] \tag{20}$$

$$\sigma_\theta = \frac{E(r)}{(1+\nu)(1-2\nu)}[(1-\nu)\varepsilon_\theta + \nu\varepsilon_r - (1-\nu)\varepsilon_\theta^p - \nu\varepsilon_r^p - \nu\varepsilon_z^p - (1+\nu)\alpha(r)T(r)] \tag{21}$$

$$\sigma_z = \nu(\sigma_r + \sigma_\theta) - E(r)\alpha(r)T(r) - E(r)\varepsilon_z^P \tag{22}$$

With the help of strain-displacement relation and substituting stresses into equilibrium equation, we have stress components in terms of radial displacement as:

$$C_1(r)\frac{d^2u}{dr^2} + C_2(r)\frac{du}{dr} + C_3(r)u + C_4(r) = 0 \tag{23}$$

where coefficients $C_1$ to $C_4$ are as follows:

$$C_1 = \frac{rE}{(1-2\nu)(1+\nu)} \tag{24}$$

$$C_2 = \frac{E\nu}{(1-\nu^2)(1-2\nu)} + \frac{E}{(1-\nu^2)} + \frac{r\frac{dE}{dr}}{(1+\nu)(1-2\nu)} \tag{25}$$

$$C_3 = \frac{-E}{r(1-\nu^2)} - \frac{\nu E}{r(1-\nu^2)(1-2\nu)} + \frac{\nu\frac{dE}{dr}}{(1-\nu^2)(1-2\nu)} \tag{26}$$

$$,C_4 = \frac{-E}{1-\nu^2}(\varepsilon_r^p - \varepsilon_\theta^p) - \frac{r\frac{dE}{dr}}{(1+\nu)(1-2\nu)}(\varepsilon_r^p + \frac{\nu}{1-\nu}\varepsilon_\theta^p + \frac{\nu}{1-\nu}\varepsilon_z^p + \frac{\alpha T(1+\nu)}{(1-\nu)})-$$

$$\frac{rE}{(1+\nu)(1-2\nu)}\left(\frac{d}{dr}\left(\varepsilon_r^p + \frac{\nu}{1-\nu}\varepsilon_\theta^p + \frac{\nu}{1-\nu}\varepsilon_z^p\right) + \frac{1+\nu}{1-\nu}\frac{d}{dr}(\alpha T)\right) \tag{27}$$

Using the same technique mentioned before, Eqs. (14) and (23) with variable coefficients for elastic and plastic deformations, respectively, can be transformed into a system of $m$ ordinary differential equations with constant coefficients. The solution for the obtained ordinary differential equation is:

$$u^k = X_1^k\exp(\lambda_1^k r) + X_2^k\exp(\lambda_2^k r) - \frac{C_4^k}{C_3^k} \tag{28}$$

where $X_1^k$ and $X_2^k$ are unknown constants for $k^{th}$ domain and

$$\lambda_1^k \quad , \quad \lambda_2^k = \frac{-C_2^k \pm \sqrt{(C_2^k)^2 - 4C_3^k C_1^k}}{2C_1^k} \tag{29}$$

The coefficients $X_1^k$ and $X_2^k$ can be determined based on continuity conditions. So, the continuity of the radial displacement $u$ and radial stress $\sigma_r$ are applied at the interfaces of the adjacent sub-domains.

$$u^k|_{r=r^k+\frac{t}{2}} = u^{k+1}|_{r=r^{k+1}-\frac{t}{2}} \tag{30}$$

$$\sigma_r^k|_{r=r^k+\frac{t}{2}} = \sigma_r^{k+1}|_{r=r^{k+1}-\frac{t}{2}} \tag{31}$$

The boundary conditions for inner and outer radii are:

$$\sigma_r(r=r_i) = -P \quad , \quad \sigma_r(r=r_o) = 0 \tag{32}$$

where $\sigma_r$ is the stress along the radius and $P$ is the internal pressure. The continuity conditions between adjacent domains together with the boundary conditions in inner and outer domains of the cylinder yield a system of $2m\times2m$ linear equations. Solving these linear equations for $X_1^k$ and $X_2^k$ in each sub-domain and then substituting these coefficients in relation (28), radial displacement is obtained. Having radial displacements, Eq. (12), we can readily generate radial and circumferential strains as follows:

$$\varepsilon_r^k = \lambda_1^k X_1^k\exp(\lambda_1^k r) + \lambda_2^k X_2^k\exp(\lambda_2^k r) \tag{33}$$

$$\varepsilon_\theta^k = \frac{X_1^k}{r}\exp(\lambda_1^k r) + \frac{X_2^k}{r}\exp(\lambda_2^k r) - \frac{C_4^k}{rC_3^k} \tag{34}$$

Finally, stresses are obtained for elastic deformation as:

$$\sigma_r^k = \frac{E^k}{(1+\nu)(1-2\nu)}\left[\left((1-\nu)\lambda_1^k + \frac{\upsilon}{r}\right)X_1^k\exp(\lambda_1^k r) + \left((1-\nu)\lambda_2^k + \frac{\upsilon}{r}\right)X_2^k\exp(\lambda_2^k r) - \frac{\upsilon C_4^k}{rC_3^k} - (1+\upsilon)\alpha^k T^k\right] \tag{35}$$

$$\sigma_{\theta}^{k} = \frac{E^{k}}{(1+\nu)(1-2\nu)}\left[\left((1-\nu)\upsilon\lambda_{1}^{k} + \frac{1}{r}\right)X_{1}^{k}\exp(\lambda_{1}^{k}r) + \left((1-\upsilon)\lambda_{2}^{k} + \frac{1}{r}\right)X_{2}^{k}\exp(\lambda_{2}^{k}r)\right] \tag{36}$$

$$\sigma_{z}^{k} = \nu(\sigma_{r}^{k} + \sigma_{\theta}^{k}) - E^{k}\alpha^{k}T^{k} \tag{37}$$

And for plastic deformation as:

$$\sigma_{r}^{k} = \frac{E^{k}}{(1+\nu)(1-2\nu)}\left[\left((1-\nu)\lambda_{1}^{k} + \frac{\upsilon}{r}\right)X_{1}^{k} + \left((1-\nu)\lambda_{2}^{k} + \frac{\upsilon}{r}\right)X_{2}^{k}\exp(\lambda_{2}^{k}r) - \frac{\upsilon C_{4}^{k}}{rC_{3}^{k}} - ((1-\nu)\varepsilon_{r}^{pk} + \upsilon\varepsilon_{\theta}^{pk} + \upsilon\varepsilon_{\theta}^{pk}) - (1+\upsilon)\alpha^{k}T^{k}\right] \tag{38}$$

$$\sigma_{\theta}^{k} = \frac{E^{k}}{(1+\nu)(1-2\nu)}\left[\left(\upsilon\lambda_{1}^{k} + \frac{1-\nu}{r}\right)X_{1}^{k} + \left(\upsilon\lambda_{2}^{k} + \frac{1-\nu}{r}\right)X_{2}^{k}\exp(\lambda_{2}^{k}r) - \frac{(1-\nu)C_{4}^{k}}{rC_{3}^{k}} - ((1-\nu)\varepsilon_{\theta}^{pk} + \upsilon\varepsilon_{r}^{pk} + \upsilon\varepsilon_{r}^{pk}) - (1+\upsilon)\alpha^{k}T^{k}\right] \tag{39}$$

$$\sigma_{z}^{k} = \nu(\sigma_{r}^{k} + \sigma_{\theta}^{k}) - E^{k}\alpha^{k}T^{k} - E^{k}\varepsilon_{z}^{pk} \tag{40}$$

## 6. Nonlinear kinematic hardening

Armstrong and Frederick (1966) suggested a refinement upon the linear kinematic hardening model. They introduced their model by adding an extra term to the Prager's rule as:

$$dX_{ij} = \frac{2}{3}Cd\varepsilon_{ij}^{p} - \gamma X_{ij}dp \tag{41}$$

where $X_{ij}$ and $dp$ are back stress (equilibrium stress) and effective plastic strain respectively. $C$ and $\gamma$ are material constants.

$$dp = \sqrt{\frac{2}{3}d\varepsilon_{ij}^{p}d\varepsilon_{ij}^{p}} \tag{42}$$

The plastic strain increment can be obtained using the following associated flow rule:

$$d\varepsilon_{ij}^{p} = d\lambda\frac{\partial f(\sigma_{ij})}{\partial\sigma_{ij}} \tag{43}$$

where $d\lambda$ is the plastic multiplier and $f$ is the von Mises yield criterion which is defined as:

$$f = J_{2}(\sigma' - X') - \sigma_{y} \tag{44}$$

$$J_{2}(\sigma' - X') = \left[\frac{3}{2}(\sigma' - X'):(\sigma' - X')\right]^{\frac{1}{2}} \tag{45}$$

where $\sigma'$ is the deviatoric stress and Eq. (45) can be expressed in cylindrical coordinates as:

$$(\sigma_{r}' - X_{r}')^{2} + (\sigma_{\theta}' - X_{\theta}')^{2} + (\sigma_{z}' - X_{r}' - X_{\theta}')^{2} = \frac{2}{3}\sigma_{y}^{2} \tag{46}$$

where $X'$ is the deviatoric back stress that defines the position of the yield surface and $\sigma_{y}$ is the initial yield stress. Normality rule can also be rewritten as:

$$d\varepsilon_{ij}^{p} = \frac{1}{k^{p}}(n_{pq}d\sigma_{pq})n_{ij} \tag{47}$$

$$n_{ij} = \frac{\partial f/\partial\sigma_{ij}}{\|\partial f/\partial\sigma_{ij}\|} \tag{48}$$

where $n_{ij}$ is the outward surface normal and $k^{p}$ proportionality factor called plastic modulus. Using consistency condition:

$$df = \frac{\partial f}{\partial\sigma_{ij}}d\sigma_{ij} + \frac{\partial f}{\partial X_{ij}}dX_{ij} = 0 \tag{49}$$

And substituting Eq. (43) into Eq. (37), $k^{p}$ is determined as:

$$k^{p} = \frac{2}{3}C - \gamma\frac{(\sigma_{ij}' - X_{ij}')X_{ij}}{\sigma_{y}} \tag{50}$$

**Table 1**
Material properties [37].

| | E (GPa) | ρ (kg/m$^3$) | α×10$^6$ (1/ °C) | K (W/m K) | υ |
|---|---|---|---|---|---|
| Metal | 200 | 7860 | 11.7 | 42 | 0.3 |
| Ceramic | 351 | 5700 | 10 | 2 | 0.3 |

## 7. Numerical method

In this investigation, return mapping algorithm (RMA) [35,36] was used to solve the plastic part of the problem. This method represents a well-established integration scheme of the elasto-plastic constitutive equations. The return mapping algorithm includes two steps: an elastic predictor and a plastic corrector. The elastic predictor leads to the so-called elastic trial error, used to formulate a concise computational loading/unloading criterion for the material. In the plastic corrector phase, a closest point projection algorithm is utilized to reinforce consistency, rendering an implicit and first-order accurate integration method [35]. The iterative method steps for computing the plastic behavior of material is presented in Appendix B.

## 8. Results

In this study, inner and outer radii of the FG cylinder are 0.17 m and 0.21 m respectively and the material properties are assumed to be independent of temperature and are listed in Table 1. We divided the total thickness into 200 sub-domains to make sure that the thickness of each sub-domain becomes too small to get higher accuracy (In fact for each sub-domain, the mean radius where the ordinary differential equations are calculated at, overlaps with its inner radius in a good approximation). The cylinder is subjected to internal pressure and cyclic temperature gradient loadings. Temperature is increased linearly and incrementally from zero temperature in a way that each increasing step is 1 °C, then when the cylinder reaches the yield point, temperature is decreased till it reaches zero value. In this situation, a cyclic loading and unloading is completed. 300 cycles (low cycle) have been applied to the cylinder to study its behavior under cyclic loading [36]. The analysis is conducted using steel as the inner surface metal and zirconia as the outer surface ceramic.

Results are presented for two different cases according to the ceramic percentage in outer radius as:

1) $n = 2$, $a = 0.989$ *(90% ceramic in the outer layer)*
2) $n = 2$,$a = 0.927$ (50% ceramic in the outer layer)

Considering non-dimensional pressure of $\frac{P}{P_y} =$ 0.8 and non-dimensional temperature of $\frac{T}{T_y} =$ 1.8, after one cycle of loading, plastic strain remains constant and does not vary by repeating the loading cycles. In this condition, cylinder behavior will be thoroughly elastic after one cycle which is denoted as elastic shakedown. Fig. 2, shows the variation of tangential stress in terms of tangential mechanical strain for this case.

Upon increasing the nondimensional temperature up to $T/T_y = 4$, it can be observed in Fig. 3, that plastic strain increases

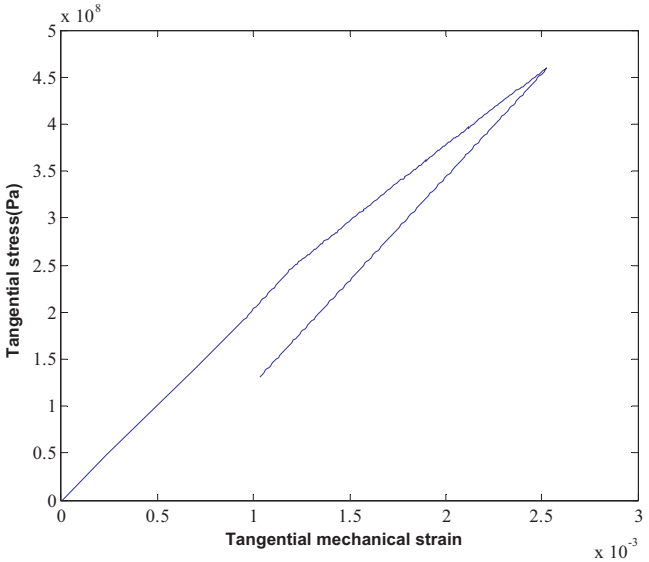


**Fig. 2.** Tangential stress in terms of tangential mechanical strain for 90% ceramic in the outer layer ($p/p_y = 0.8 \quad and T/T_y = 1.8$).

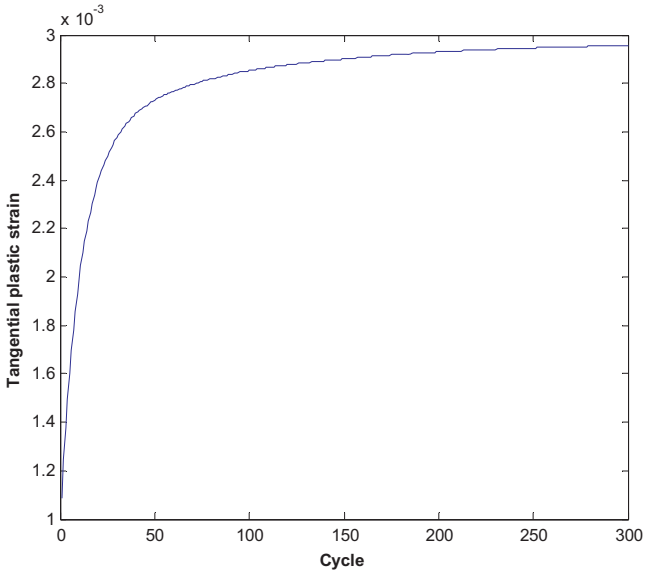


**Fig. 3.** Tangential plastic strain in terms of cycle for 90% ceramic in the outer layer ($p/p_y = 0.8 \quad and T/T_y = 4$).

continuously by increasing cycles. This phenomenon is called ratcheting which is a non-safe domain. Fig. 4. illustrates tangential stress, the dominant stress in ratcheting domain, versus tangential mechanical strain. For ratcheting case, the loop doesn't close and stabilize.

Now, Bree's interaction diagram can be obtained for different temperatures and pressures to study the behavior of the material. As we see from Figs. 5 and 6, the boundaries between each domain is specified based on the behavior of each point in specific temperature and pressure.

## 9. Conclusion

In the present paper, the elastoplastic analysis on a FG thick-walled cylinder subjected to constant internal pressure has been done to study how the cylinder behaves under cyclic thermo-mechanical loading. A model of nonlinear kinematic hardening based on

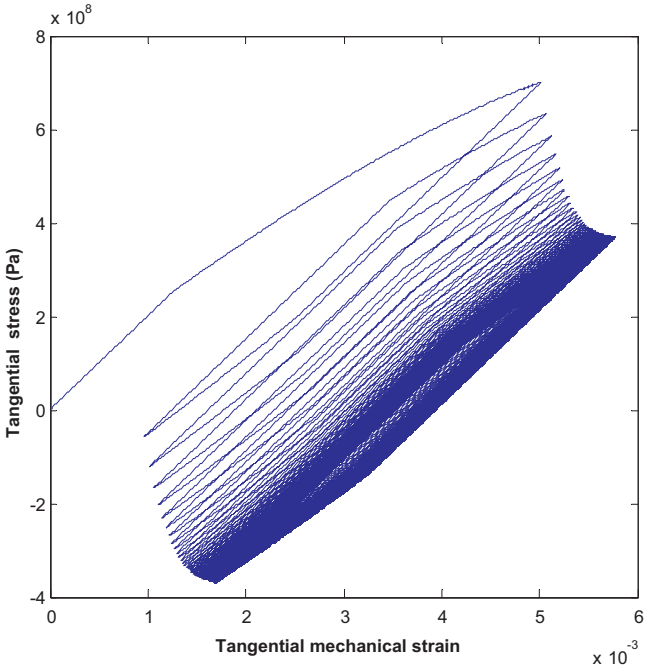


**Fig. 4.** Tangential stress in terms of tangential mechanical strain for 90% ceramic in the outer layer ($p/p_y = 0.8 \quad and T/T_y = 4$).

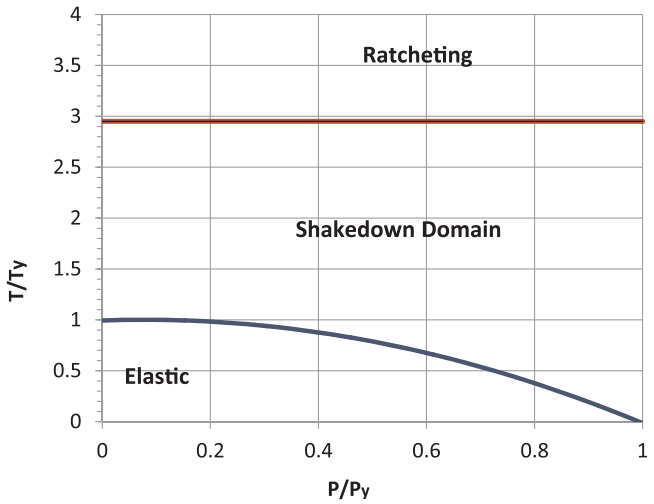


**Fig. 5.** The Bree's diagram (90% ceramic in the outer layer).

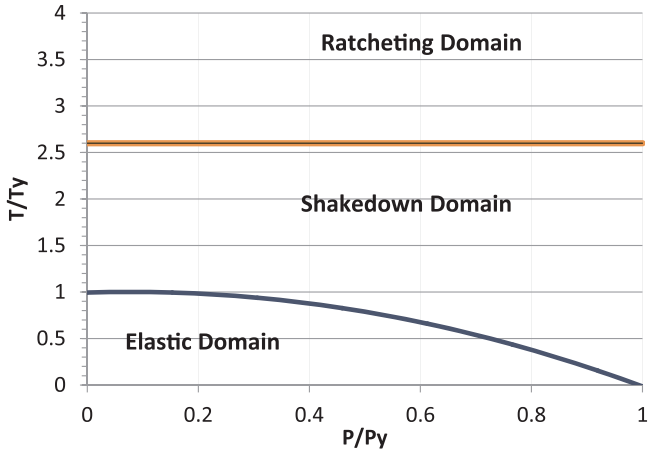


**Fig. 6.** The Bree's diagram (50% ceramic in the outer layer).

Armstrong and Frederick was used. Return mapping algorithm was employed to get the plastic strains increments. The presented Bree's diagram is capable of demonstrating the safe boundary of loading for different temperatures and pressures. Dividing the Bree's diagram into three regions, it can be deduced that reducing the amount of ceramic in the outer layer can change the boundary between shakedown and ratcheting domain that results in enlarging the ratcheting domain and subsequently lowering the loading capacity and failure is more likely to happen then. The optimal design must be under the ratcheting domain.

**Acknowledgements**

We thank Dr. Nayebi for sharing his comments that greatly improved the manuscript, and we also thank 3 “anonymous” reviewers for their so-called insights.

**Conflict of interest**

The author(s) declared no potential conflicts of interest with respect to the research, authorship, and/or publication of this article.

**Appendix A. Notation**

| | | | |
|---|---|---|---|
| $B$ | Typical material property | $u$ | Radial displacement field |
| $V$ | Volume fraction | $\upsilon$ | Poisson's ratio |
| $n$ | Gradient index | $P$ | Internal pressure |
| $r_{in}$ | inner radius | $E$ | Young Modulus |

| | | | |
|---|---|---|---|
| $r_{out}$ | Outer radius | $X_{ij}$ | Back stress (equilibrium stress) |
| $K$ | Heat conductivity | $X'$ | Deviatoric back stress |
| $T_i$ | Temperature of inner surface | $dp$ | Effective plastic strain |
| $T$ | Temperature distribution | $c$ | Material constant |
| $k$ | Number of division | $\gamma$ | Material constant |
| $t$ | Radial width of each sub-domain | $d\varepsilon_{ij}^{p}$ | Plastic strain increment |
| $\sigma_r$ | Radial stress | $\sigma'$ | Deviatoric stress |
| $\sigma_\theta$ | Circumferential stress | $\sigma_Y$ | Initial yield stress |
| $\sigma_z$ | Longitudinal stress | $k^p$ | plastic modulus |
| $\varepsilon_r$ | Radial strain | $P_y$ | Yield pressure |
| $\varepsilon_\theta$ | Circumferential strain | $T_y$ | Yield temperature |
| $\varepsilon_z$ | Longitudinal strain | $\alpha$ | Coefficient of thermal expansion |
| $\rho$ | Density | $f$ | Yield function |

## Appendix B

1) The cylinder thickness is divided into m sub-domains.
2) Stresses and strains are determined for a pressure below the yield pressure. ($\sigma_{ij}^{total} = \sigma_{ij}^{p}$)
3) Thermal loading is divided into N steps.
4) Variables of total and incremental plastic strain and accordingly those of total and incremental back stress are assumed to be zero. ($d\varepsilon_{ij}^{p} = 0$, $dX_{ij} = 0$)
5) Elastic stress is determined for one-step thermal loading considering $p = 0$. ($d\sigma_{ij}^{\Delta L}$)
6) For total stress ($\sigma_{ij}^{total} = \sigma_{ij}^{total} + d\sigma_{ij}^{\Delta L}$), yield surface function and relation ($n_{pq} d\sigma_{pq}$) are calculated for each sub-domain.
7) If for each domain <0, elastic loading status has been occurred.
8) If for each sub-domain $f$>0 and ($n_{pq} d\sigma_{pq}^{\Delta L}$) > 0, plastic loading status will occur for that sub-domain, which then plastic correction step will be applied.
9) Using normality relation, $d\varepsilon_{ij}^{p}$ is determined for plastic sub-domains and then $dX_{ij}$ is determined for all plastic sub-domains.
10) Having $d\varepsilon_{ij}^{p}$ for plastic sub-domains and $d\varepsilon_{ij}^{p} = 0$ for elastic ones, stresses ($d\sigma_{ij}^{\Delta L}$) are determined in each layer.
11) Considering total stress $s_{ij}^{total} = s_{ij}^{total} + ds_{ij}^{DL}$ and total back stress ($X_{ij} = X_{ij} + dX_{ij}$), yield surface function is investigated. If for all plastic sub-domains $\frac{f}{s_y^2}$<0.01, plastic correction has been done and we return to step (5), otherwise return to step (9) in order to determine new $d\varepsilon_{ij}^{p}$
12) Steps (9)–(11) are repeated until $\frac{f}{s_y^2}$<0.01 is applied for all plastic sub-domains of cylinder simultaneously.
13) ($de_{ij}^{pN} = de_{ij}^{p}$),$deX_{ij}^{N} = dX_{ij}$

## References


[1] H.S. Shen, Functionally Graded Materials: Nonlinear Analysis of Shells and Plates, CRC Press, USA, 2009.
[2] M. Jafari, G. Atefi, J. Khalesi, et al., A new conjugate heat transfer method to analyse a 3D steam cooled gas turbine blade with temperature-dependent material properties, Proc. IMechE Part C: J. Mech. Eng. Sci. 226 (2012) 1309–1320.
[3] M. Jafari, G. Atefi, J. Khalesi, Advances in nonlinear stress analysis of a steam cooled gas turbine blade, Lat. Am. Appl. Res. 42 (2012) 167–175.
[4] M.H. Jalali, O. Zargar, M. Baghani, Iran. J. Sci. Technol. Trans. Mech. Eng. (2018), https://doi.org/10.1007/s40997-018-0193-6.
[5] M.H. Jalali, B. Shahriari, O. Zargar, M. Baghani, M. Baniassadi, Free vibration analysis of rotating functionally graded annular disc of variable thickness using generalized differential quadrature method, Sci. Iran. 25 (2017) 728.
[6] A.R. Khoei, B. Bahmani, Comput. Mech. (2018), https://doi.org/10.1007/s00466-018-1555-z.
[7] Y. Sun, L. Shi-Rong, R.C. Batra, Thermal buckling and post-buckling of FGM Timoshenko beams on nonlinear elastic foundation, J. Therm. Stress. 39 (2016) 11–26.
[8] E. Hosseini, S.R. Holdsworth, U. Flueeler, A temperature-dependent asymmetric constitutive model for cast irons under cyclic loading conditions, J. Strain Anal. Eng. 53 (2) (2017) 106–114.
[9] B. Safaei, R. Moradi-Dastjerdi, F. Chu, Effect of thermal gradient load on thermo-elastic vibrational behavior of sandwich plates reinforced by carbon nanotube agglomerations, Compos. Struct. 192 (2018) 28–37, https://doi.org/10.1016/j.compstruct.2018.02.022.
[10] D.B. Bland, Elastoplastic thick-walled tubes of work hardening material subjected to internal and external pressures and to temperature gradients, J. Mech. Phys. Solids 4 (4) (1956) 209–229.
[11] M.G. Derington, The onset yield in a thick cylinder subjected to uniform internal or external pressure and steady state heat flow, Int. J. Mech. Sci. 4 (1) (1982) 83–103.
[12] Y. Fukui, N. Yamanaka, Elastic analysis for thick-walled tubes of functionally graded material subjected to internal pressure, JSME Int. J. 35 (4) (1992) 379–385 (Series 1).
[13] Y. Obata, N. Noda, Steady thermal stresses in a hollow circular cylinder and a hollow sphere of a functionally gradient material, J. Therm. Stress. 17 (3) (1994) 471–487.
[14] A. Loghman, M.A. Wahab, Loading and unloading of thick-walled cylindrical pressure vessels of strain-hardening material, J. Press. Vessel Technol. 116 (2) (1994) 105–109.
[15] M.P. Lutz, R.W. Zimmerman, Thermal stresses and effective thermal expansion coefficient of a functionally gradient sphere, J. Therm. Stress. 19 (1) (1996) 39–54.
[16] R.W. Zimmerman, M.P. Lutz, Thermal stresses and thermal expansion in a uniformly heated functionally graded cylinder, J. Therm. Stress. 22 (2) (1999)

177–188.
[17] Y.M. Shabana, N. Noda, Thermo-elasto-plastic stresses in functionally graded materials subjected to thermal loading taking residual stresses of the fabrication process into consideration, Compos. Part B: Eng. 32 (2) (2001) 111–121.
[18] N. Tutuncu, M. Ozturk, Exact solutions for stresses in functionally graded pressure vessels, Compos. Part B: Eng. 32 (8) (2001) 683–686.
[19] A. Nayebi, R. El Abdi, Cyclic plastic and creep behaviour of pressure vessels under thermomechanical loading, Comput. Mater. Sci. 25 (3) (2002) 285–296.
[20] A. Oral, G. Anlas, Effects of radially varying moduli on stress distribution of nonhomogeneous anisotropic cylindrical bodies, Int. J. Solids Struct. 42 (20) (2005) 5568–5588.
[21] A. Safari, M. Tahani, S.M. Hosseini, Two-dimensional dynamic analysis of thermal stresses in a finite-length FG thick hollow cylinder subjected to thermal shock loading using an analytical method, Acta Mech. 220 (2011) 299–314.
[22] L.H. You, H. Ou, Z.Y. Zheng, Creep deformations and stresses in thick-walled cylindrical vessels of functionally graded materials subjected to internal pressure, Compos. Struct. 78 (2) (2007) 285–291.
[23] J.N. Reddy, C.D. Chin, Thermomechanical analysis of functionally graded cylinders and plates, J. Therm. Stresses 21 (6) (1998) 593–626.
[24] J.J. Chen, S.T. Tu, F.Z. Xuan, Z.D. Wang, Creep analysis for a functionally graded cylinder subjected to internal and external pressure, J. Strain Anal. Eng. Des. 42 (2) (2007) 69–77.
[25] K. Abrinia, H. Naee, F. Sadeghi, F. Djavanroodi, New analysis for the FGM thick cylinders under combined pressure and temperature loading, Am. J. Appl. Sci. 5 (7) (2008) 852–859.
[26] H. Darijani, M.H. Kargarnovin, R. Naghdabadi, Design of thick-walled cylindrical vessels under internal pressure based on elasto-plastic approach, Mater. Des. 30 (9) (2009) 3537–3544.
[27] X.L. Peng, X.F. Li, Thermoelastic analysis of a cylindrical vessel of functionally graded materials, Int. J. Press. Vessels Pip. 87 (5) (2010) 203–210.
[28] A. Parvizi, R. Naghdabadi, J. Arghavani, Analysis of Al A359/SiCp functionally graded cylinder subjected to internal pressure and temperature gradient with elastic-plastic deformation, J. Therm. Stress. 34 (10) (2011) 1054–1070.
[29] Y. Bayat, M. Ghannad, H. Torabi, Analytical and numerical analysis for the FGM thick sphere under combined pressure and temperature loading, Arch. Appl. Mech. 82 (2) (2012) 229–242.
[30] T. Singh, H. Singh, Steady state creep behavior of functionally graded thick cylinder, World Acad. Sci. Eng. Technol. Int. J. Mech. Aerosp. Ind. Mechatron. Manuf. Eng. 7 (12) (2013) 2499–2505.
[31] A. Nayebi, A. Tirmomenin, M. Damadam, Elasto-plastic analysis of a functionally graded rotating disk under cyclic thermo-mechanical loadings considering continuum damage mechanics, Int. J. Appl. Mech. 7 (02) (2015) 1550026.
[32] M.R. Nami, M. Janghorban, M. Damadam, Thermal buckling analysis of functionally graded rectangular nanoplates based on nonlocal third-order shear deformation theory, Aerosp. Sci. Technol. 41 (2015) 7–15.
[33] E. Mahdavi, A. Ghasemi, R.A. Alashti, Elastic–plastic analysis of functionally graded rotating disks with variable thickness and temperature-dependent material properties under mechanical loading and unloading, Aerosp. Sci. Technol. 59 (2016) 57–68.
[34] A. Loghman, A.G. Arani, A.R. Shajari, S. Amir, Time-dependent thermoelastic creep analysis of rotating disk made of Al–SiC composite, Arch. Appl. Mech. 81 (12) (2011) 1853–1864.
[35] P.K.V. Nukala, A return mapping algorithm for cyclic viscoplastic constitutive models, Comput. Methods Appl. Mech. Eng. 195 (1) (2006) 148–178.
[36] O.S. Hopperstad, S. Remseth, A return mapping algorithm for a class of cyclic plasticity models, Int. J. Numer. Methods Eng. 38 (4) (1995) 549–564.
[37] M. Bayat, M. Saleem, B.B. Sahari, A.M.S. Hamouda, E. Mahdi, Analysis of functionally graded rotating disks with variable thickness, Mech. Res. Commun. 35 (5) (2008) 283–309.